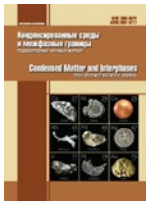

ISSN 1606-867X (Print)
ISSN 2687-0711 (Online)
Конденсированные среды и межфазные границы
https://journals.vsu.ru/kcmf/

Original articles

Research article
https://doi.org/10.17308/kcmf.2026.28/13820

Pressure-dependent linewidth and Grüneisen parameter calculated from the soft Raman mode in zirconia

N. Kara[1], A. Kiraci[2]✉ and H. Yurtseven[3]

[1]Middle East Technical University, Ankara 06790, Turkey

[2]Intercurricular Courses Department, Cankaya University, Ankara 06790, Turkey

[3]Department of Computer Engineering, Baskent University, Ankara 06790, Turkey

Abstract

Objectives: The halfwidth at half maximum (HWHM or linewidth) of the soft Raman E_g mode at 260 cm^{-1} in Zirconia (ZrO_2) was quantitatively interpreted as a function of pressure at room temperature using the Ising pseudospin-phonon coupled model predictions, namely the pseudospin-phonon coupled (PS) the energy fluctuation (EF) models.

Experimental: The soft Raman E_g mode frequency, associated to the order parameter, is used to determine the inverse of relaxation time as a function of pressure in ZrO_2. Furthermore, the activation energy calculation for ZrO_2 was carried out from our obtained values of HWHM from both PS and EF models. Moreover, the temperature dependence of this E_g mode was predicted through the two models studied here. Finally, the volume-pressure phase diagram of zirconia from the literature was used to estimate the isothermal Grüinesen parameter of the Raman modes at 150, 260, 320, 480, 602, and 650 cm^{-1} of ZrO_2 as a function of pressure.

Conclusions: Our results indicate that both the PS and EF models adequately describe the increasing and decreasing behavior of the observed HWHM as a function of pressure and temperature, respectively for the soft Raman E_g mode in ZrO_2.

Keywords: Linewidth, Grüniesen parameter, Raman frequency, ZrO_2

For citation: Kara N., Kiraci A., Yurtseven H. Pressure-dependent linewidth and Grüneisen parameter calculated from the soft Raman mode in zirconia. *Condensed Matter and Interphases*. 2026;28(3): 363–375. https://doi.org/10.17308/kcmf.2026.28/13820

✉ Kiraci A., e-mail: akiraci@cankaya.edu.tr
© Kara N., Kiraci A., Yurtseven H., 2026

Контент доступен под лицензией Creative Commons Attribution 4.0 License.

Оригинальные статьи

Научная статья
https://doi.org/10.17308/kcmf.2026.28/13820

Зависимость ширины линии и параметра Грюнайзена от давления, рассчитанная по мягкой моде комбинационного рассеяния света в диоксиде циркония

Н. Кара[1], А. Кирачи[2]✉, Х. Юртсевен[3]

[1] *Ближневосточный технический университет, Анкара 06790, Турция*

[2]*Кафедра межфакультетских курсов, Университет Чанкая, Анкара 06790, Турция*

[3]*Кафедра компьютерной инженерии, Башкентский Университет, Анкара 06790, Турция*

Аннотация

Цель статьи: В рамках предсказаний моделей связи псевдоспина и фононов (а именно: модели связи псевдоспина и фононов [PS] и модели флуктуаций энергии [EF]) проведена количественная интерпретация полуширины на полувысоте (HWHM, или ширины линии) мягкой E_g-моды комбинационного рассеяния (КР) при 260 см$^{-1}$ в диоксиде циркония (ZrO_2) как функции давления при комнатной температуре.

Экспериментальная часть: Частота мягкой E_g-моды КР, связанная с параметром порядка, была использована для определения обратного времени релаксации в зависимости от давления в ZrO_2. На основе полученных значений полуширины (HWHM) в рамках обеих моделей (PS и EF) выполнен расчет энергии активации для ZrO_2. С помощью двух исследуемых моделей также предсказана температурная зависимость частоты данной E_g-моды. Наконец, литературные данные по *p-V* фазовой диаграмме диоксида циркония были использованы для оценки барической зависимости изотермического параметра Грюнайзена КР-мод с частотами 150, 260, 320, 480, 602 и 650 см$^{-1}$ в ZrO_2.

Выводы: Полученные результаты показывают, что обе модели (PS и EF) адекватно описывают наблюдаемое изменение полуширины (HWHM) мягкой E_g-моды комбинационного рассеяния света в ZrO_2 при варьировании давления и температуры соответственно.

Ключевые слова: ширина линии, параметр Грюнайзена, рамановская частота, ZrO_2

Для цитирования: Кара Н., Кирачи А., Юртсевен Х. Зависимость ширины линии и параметра Грюнайзена от давления, рассчитанная по мягкой моде комбинационного рассеяния света в диоксиде циркония. *Конденсированные среды и межфазные границы*. 2026;28(3): 363–375. https://doi.org/10.17308/kcmf.2026.28/13820

✉ Али Кирачи, e-mail: akiraci@cankaya.edu.tr
© Кара Н., Кирачи А., Юртсевен Х., 2026

1. Introduction

Wear resistance, low volatility, extraordinary mechanical strength, refractoriness, low thermal conductivity, high chemical resistance, and biological inertness are just a few of the remarkable properties of zirconium dioxide (zirconia, ZrO_2) and materials based on it, which exhibit complex polymorphism including high-pressure and high-temperature phases [1]. This material has also been reported [2] to be utilized in engineering ceramics for high-temperature equipment, oxygen sensors and thermal barriers. Five distinct forms of zirconia have been reported, all of which have been thoroughly described via crystallography [3–9]. While the two orthorhombic *Pbca* and *Pnma* polymorphs (respectively, isostructural to brookite TiO_2 and to cotunnite $PbCl_2$) are stable between 3–5 GPa and 12.5–20 GPa and above 12.5–20 GPa, the monoclinic (baddeleyite $P2_1/c$, below 1500 K), tetragonal $P4_2/nmc$ (between 1500 and 2650 K), and cubic $Fm\bar{3}m$ (isostructural to fluorite CaF_2 above 2650 K) polymorphs are stable at room pressure. At ambient conditions, ZrO_2 is reported to be in monoclinic phase with the space group C_{2h}^5 or $P2_1lc$ [10]. As the temperature increases, a first-order displacive martensitic phase transition to a tetragonal structure with a space group D_{4h}^{15} or $P4_2/nmc$ has been considered to take place at around 1400 K [11]. A phase transition

from tetragonal to cubic fluorite structure with a space group O_h^5 or $Fm3m$ has been indicated [12] at a temperature about 2600 K. On the other hand, a pressure-induced phase transition from monoclinic to orthorhombic phase (Ortho I) is reported for the pressure range of 3–11 GPa [13–15]. Another pressure-induced phase transition from Ortho I to Ortho II was observed in the range of 9–15 GPa [14].

Numerous theoretical and experimental investigations on zirconia and its derivative materials have been documented in the literature. Using first-principles techniques, the thermoelastic, vibrational, structural, and dielectric characteristics of the most prevalent zirconia polymorphs at room pressure have been examined for the cubic, tetragonal, and monoclinic ZrO_2 phases [16, 17–23]. Using density-functional perturbation theory, the structural parameters and phonon spectra of the five known zirconia polymorphs have been calculated at pressures up to 48 GPa in both the local-density and the generalized gradient approximations by Fadda et al. [24]. They have performed phonon calculations to extract dielectric characteristics such as the lattice contribution and the Raman spectra, and thermoelastic properties in the quasiharmonic approximation such as Grüneisen mode parameters. Gorelov has discussed the high-temperature phase transition in ZrO_2 [1]. Block et al. used X-ray diffraction and optical microscopy to determine the pressure-temperature phase diagram of zirconia [25]. The results of hydrostatic high-pressure XRD experiments were used by Bouvier et al. to document the high-pressure structural evolution of undoped tetragonal monocrystalline zirconia [26]. Ji-Hoon Park et al. [27] described the phase transition and thermal expansion properties of zirconia and its modifications. Additionally, Bouvier and Lucazeau acquired Raman spectra and vibrational analysis of nanometric tetragonal zirconia under high pressure using an XY Dilor multichannel spectrometer connected with a CCD detector [28]. In order to create "stabilized zirconia," the high temperature phases of ZrO_2 can be stabilized at room temperature and pressure by replacing some of the zirconium with magnesium, calcium, cerium, or yttrium. In their study, Li et al. [29] have compared the phonons in 8 mol % yttrium-stabilized tetragonal zirconia (YSZ) and monoclinic zirconia (ZrO_2) from room temperature to 1373 K using density functional theory (DFT), inelastic neutron scattering spectrometry, and Raman spectrometry. It has been established that temperature, pressure, and grain size all play significant roles in the oxidation process and in stabilizing the tetragonal form at the metal/oxide interface. In particular, the impact of nanocrystallite size on the pressure-temperature phase diagram of zirconia produced by oxidation of zirconium-based alloys has been investigated by Bouvier et al. [30].

Using the critical behavior of the soft mode as an order parameter, we estimated the pressure dependence of the frequency, damping constant, inverse relaxation time and activation energy in ZrO_2. The soft-mode frequency (ω) and intensity of the soft-phonon mode decrease to zero ($\omega \to 0$) when the pressure P approaches the transition pressure of P_C in ZrO_2, as reported earlier [19]. It is of interest to determine the pressure dependence of the soft-mode frequency (ω) and then predict its HWHM (linewidth), activation energy, and inverse relaxation time as functions of pressure in this material. This motivates us to study the critical behavior of Raman mode frequency (ω) and its HWHM (linewidth) in ZrO_2 below P_C. Therefore, as an order parameter ($P < P_C$), we compute the pressure dependency of the frequency (ω) in the current study. Additionally, we calculate the activation energy, the inverse relaxation time and the linewidth as a function of pressure below P_C in this material. As in our earlier research works, we employ the energy-fluctuation (EF) and the pseudospin-phonon coupled (PS) models. Both models are given in detail in the theory part to calculate the linewidth [31–36]. Finally, the linewidth of the E_g Raman soft mode was predicted as a function of temperature from the pressure dependence of its observed [28] linewidth using the pressure-temperature phase diagram of ZrO_2 from the literature for both the monoclinic-tetragonal II and orthorhombic I – orthorhombic II transition pressures of P_C = 3.3 and 20.1 GPa, respectively.

The "Theory" is given in section 2. The "Calculation and Result" and the "Discussion" parts are given in section 3 and 4, respectively. Our "Conclusion" part is given in section 5.

2. Theory

Near phase transitions, the temperature dependence of the phonon frequencies and their linewidths can be investigated. Yamada et al.'s Ising pseudospin-phonon coupled model has been used to study those phonon modes that are linked to phase transitions [37]. The effective pair interaction $J_{eff}(\vec{r}_{ij})$ between the nearest-neighbor spins has been described using the Yamada Hamiltonian as follows:

$$H = \frac{1}{2}\sum_{\vec{k}s}(P_{\vec{k}s}P_{\vec{k}s}^{*} + \omega_{\vec{k}s}^{2}Q_{\vec{k}s}Q_{\vec{k}s}^{*}) + \sum_{ij}J_{eff}(\vec{r}_{ij})\sigma_i\sigma_j \quad (1)$$

In Eq. (1), and are the phonon's momentum and coordinate, respectively, and $\omega_{\vec{k}s}$ is the phonon's frequency for the *s* mode with the wavevector $\vec{k}$. The spin variable that corresponds to the phonon is represented by. The nearest-neighbor spin-spin, phonon-phonon, and pseudospin-phonon coupling interactions are therefore represented by this Hamiltonian. By accounting for the interactions of multiple pseudospins as well as phonons, Matsushita [38] developed the Hamiltonian of Yamada et al. (Eq. 1) to determine the temperature dependence of the damping constant (linewidth) and soft-mode frequency (in terms of the order parameter) in ammonium halides, specifically NH_4Br and NH_4Cl. Matsushita [38] obtained the mathematical equations for the phonon frequency from his Hamiltonian that reads as

$$\omega^2 = \bar{\omega}_0^2(\vec{k}\upsilon,\omega) + K_1(\vec{k},q=0,\upsilon\upsilon')\langle\sigma(\vec{q}=0)\rangle + \\ +\sum_{\vec{q}}K_2(\vec{k},\vec{q},-\vec{q},\upsilon\upsilon')\langle|\sigma(\vec{q})|^2\rangle + \mathrm{Re}\sum_{sp}(\vec{k}\upsilon,\omega) \quad (2)$$

and in particular, the damping constant associated with the dynamic scattering function $S(\vec{q},\omega)$ is expressed as follows:

$$S(\vec{q},\omega) = \int \exp(i\omega t)\sigma(\vec{q},t)\sigma^{*}(\vec{q},0)dt \quad (3)$$

The coupling between two phonons ($k\upsilon$) and ($k\upsilon'$) and the pseodospin with the wavevector $\vec{q}$ is represented by K_1 in Eq. (2). The interaction between two pseudospins ($\vec{q}$ and $-\vec{q}$). and two phonons ($k\upsilon$ and $k\upsilon'$) is defined by the coupling constant K_2. Therefore, the dynamic scattering function (Eq. 3) controls the abnormal behavior of the damping constant (linewidth) at the transition temperature (T_C). Laulicht and Luknar [39] estimated the temperature dependence of the linewidth $\Gamma_{SP}(\vec{k}\upsilon,\omega)$ that Matsushita obtained from his Hamiltonian by taking into account the peak frequency at T_C where the dynamic scattering function (Eq. 3) diverges. Temperature dependence of the damping constant was obtained due to the pseudospin-phonon coupling denoted as Γ_{SP} in the PS model. A different method for Γ_{SP} was based on Schaack and Winterfeldt's energy fluctuation near T_C (EF model) [40]. For the ferroelectric KDP material, those two models have already been examined [39,41]. The order parameter $\sigma(\vec{q}=0)=S$, as stated by Matsushita [38], is included in both formulations for Γ_{SP}. Yurtseven and Karacali [42] used Yamada's [37] Ising pseudospin-phonon coupled model (Eq. 1) and the temperature dependence of the soft mode frequency (Eq. 2), with the Matsushita's damping constant, to derive the following expressions for Γ_{SP} [40,43]: The PS model states that the damping model's temperature dependence is provided by

$$\Gamma_{SP} = \Gamma_0 + A(1-S^2)\ln\left[\frac{T_C}{T - T_C(1-S^2)}\right] \quad (4)$$

and the EF model gives

$$\Gamma_{SP} = \Gamma_0' + A'\left[\frac{T(1-S^2)}{T - T_C(1-S^2)}\right]^{1/2} \quad (5)$$

In Eqs. (4) and (5), Γ_0 (Γ_0') and A (A') represent the background damping constant and amplitude, respectively, while T_C represents the critical temperature. In both models (PS and EF), the temperature dependence of frequency ω for phonon modes due to phase transitions can be related with the order parameter *S*. The PS and EF models (Eqs. 4 and 5) can forecast the temperature dependence of a phonon mode's linewidth, Γ based on its frequency.

The activation energy U can additionally be calculated using the relation [44,45] based on the temperature dependence of the damping constant (Γ) as

$$\Gamma = \Gamma_{vib} + C\exp(-U/k_BT) \quad (6)$$

where C is a constant, k_B is the Boltzmann constant and Γ_{vib} is the vibrational relaxation which is very small close to T_C ($\Gamma_{vib} \cong 0$). Then, close to T_C, Eq. (6) provides

$$\Gamma = C\exp(-U/k_BT) \quad (7)$$

or

$$\ln\Gamma \cong -U/k_BT \quad (8)$$

The temperature dependence of the inverse relaxation time (τ^{-1}) can be determined by utilizing the soft-mode frequency and the damping constant Γ_{sp} obtained from the PS and EF models (Eqs. 4 and 5) according to

$$\tau^{-1} = \omega^2/\Gamma \quad (9)$$

Variations in the crystal's volume (V) with temperature are mainly the cause of the temepreture dependence of the phonon modes. This connection defines the mode Grüneisen parameter of those phonon modes with the frequency ω:

$$\gamma = -\frac{d\ln\omega}{d\ln V} \quad (10)$$

The pressure dependence of the isothermal mode Grüneisen parameter or mode Grüneisen parameter at constant temperature, can be defined as

$$\gamma_T(P) = -\frac{V(P)}{\omega(P)}\frac{\left(\frac{\partial\omega}{\partial P}\right)_T}{\left(\frac{\partial V}{\partial P}\right)_T} \quad (11)$$

3. Calculations and results

3.1 Calculations of the soft frequency, linewidth, inverse relaxation time and the activation energy as a function of pressure

As previously mentioned, the pseudospin-phonon coupled (PS) and the energy-fluctuation (EF) models were used to compute the linewidth Γ for the soft-phonon mode with the Raman frequency (260 cm^{-1}) as a function of pressure. For this calculation of the linewidth Γ as a function of pressure through Eqs. (4) and (5), we need not only the pressure dependence of the order parameter (S), but also the pressure (P)– temperature (T) relations (P-T phase diagram) of the ZrO_2 crystal.

For the former one, a power-law formula, $\omega^2 = a(P_C - P)^b$, has been represented to characterize the frequency softening of this soft Raman mode with a = 1916 cm^{-1}/GPa, P_C = 38.03 GPa, and b = 0.945, which we use as given previously [28] . This frequency of the soft E_g mode was associated with the order parameter (S) below P_C in ZrO_2 in this study as

$$\frac{\omega}{\omega_{\max}} \equiv S \quad (12)$$

The soft mode (E_g) frequency (squared) as a function of pressure was given in Fig. 1. For the latter one, the monoclinic (M) – tetragonal II (T-II), and the tetragonal I (T-I) – tetragonal II (T-II) transitions have been reported [25] as given, respectively, according to

$$T_C = 2025.6 - 526.3P \quad (13)$$

and

$$T_C = 832 - 13.5P \quad (14)$$

On the other hand, for the orthorhombic I (O-I)- orthorhombic II (O-II) transitions, we extracted the following relation by analyzing the observed T-P data [26] as

$$T_C = 3787.7 - 173.6P \quad (15)$$

Fig. 2 gives our extracted linear relation from the observed [26] data for both O I – O II transitions. By replacing Eq. (12) and also Eqs. (13–15) in Eqs. (4) and (5), we were able to calculate the linewidth Γ for the soft-phonon mode E_g (260 cm^{-1}) as a function of pressure. Our calculated values of Γ were then fitted to the observed data [28] and the values of the background damping constants Γ_0 (Γ_0') with

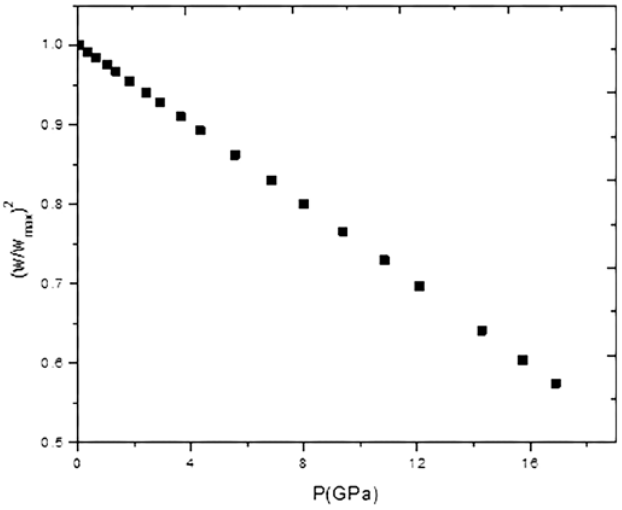

Fig. 1. Pressure dependence of the soft Raman frequency (order parameter) calculated according to $\omega^2 = 1916\ (38.03 - P)^{0.945}$ for the soft E_g mode (260 cm^{-1}) in ZrO_2

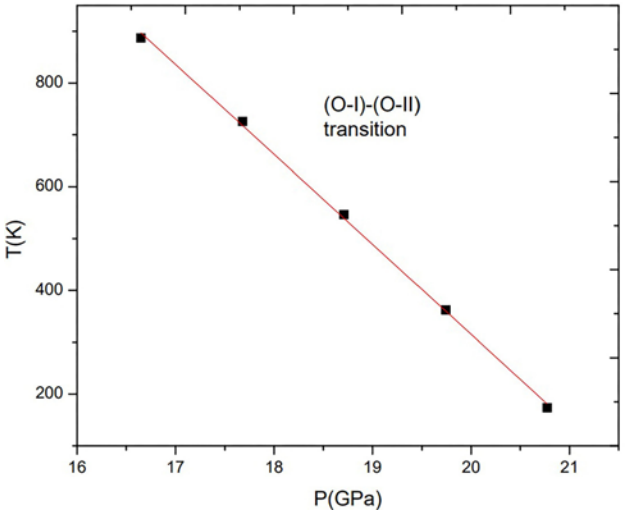

Fig. 2. Temperature-pressure phase diagram of (O-I) – (O-II) transition in ZrO_2 according to Eq. (15) using the observed [26] data

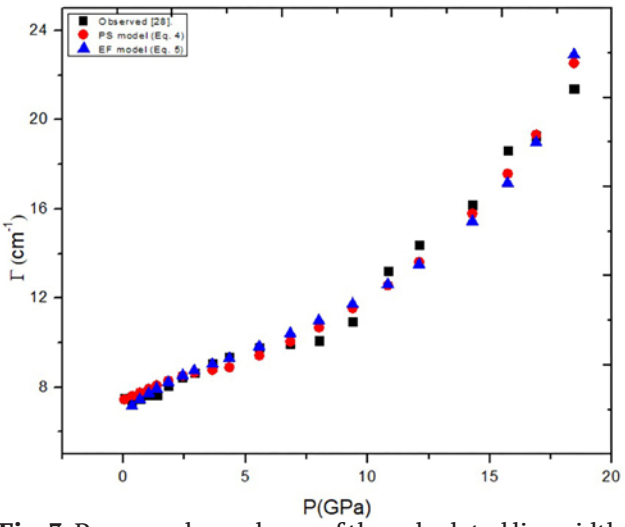

Fig. 3. Pressure dependence of the calculated linewidth Γ_{SP} using the PS (Eq. 4) and the EF (Eq. 5) models of the soft E_g mode in ZrO_2. The observed linewidth data [28] are also given here. Curve is shown as a guide to the eye

the amplitudes A (A') of Eqs. (4) and (5) (PS and EF models, respectively) were deduced for the pressure intervals indicated, as given in Table 1. In Fig.3, we present the linewidth Γ estimated as a function of pressure using Eqs. (4) and (5) with the fitted parameters (Table 1) for the E_g Raman mode in ZrO2. This figure (Fig.3) also shows the observed linewidth [28] for this Raman mode.

An Arrhenius plot of $\ln\Gamma$ against $1/T_C$ led us to extract the values of the activation energy U according to Eq. (8), as given in Fig. 4.

Our deduced values of U has been tabulated in Table 2 for the pressure intervals indicated. The pressure dependence of the inverse relaxation time τ^{-1} of this soft E_g mode (260 cm^{-1}) has been calculated according to Eq. (9) via our obtained values of linewidth from both PS and EF models, as given in Fig. 5.

The isothermal Grüneisen parameter γ_T of the Raman modes in ZrO_2 (150, 260, 320, 480, 602, and 650 cm^{-1}) was computed according to Eq. (11). In order to make this computation, the observed Raman frequency (ω) data [28] and the observed volume (V) data [26] as a function of pressure, were analyzed respectively, according to

$$\omega = a_0 + a_1 P + a_2 P^2 \quad (16)$$

and

$$V = b_0 + b_1 P + b_2 P^2 \quad (17)$$

The plots from the analysis of ω and V (Eqs. 16 and 17) are given in Fig. 6 and 7, respectively.

Table 1. Values of the damping constant Γ_0 (Γ_0') and the amplitude A (A') due to the PS (Eq. 4) and EF (Eq. 5) models for the soft E_g mode in ZrO_2 within the pressure interval $0 \le P \le 18.4$ GPa

Crystal	Raman mode	Model	Γ_0 (Γ_0') (cm^{-1})	A (A') (cm^{-1})
ZrO_2	E_g (260 cm^{-1})	PS (Eq. 4)	7.459	10.562
		EF (Eq. 5)	6.496	7.254

Table 2. Values of the activation energy U extracted from Eq. (8) due to the Raman modes indicated by using the pseudospin-phonon coupled (PS) model and the energy fluctuation (EF) model in ZrO_2

Raman Modes	Pressure interval (GPa)	$-U$ (meV) PS (Eq. 4)	$-U$ (meV) EF (Eq. 5)
E_g	0–1 < P < 84	48	71
	2.42 <P < 3.64	8	15
	4.33 < P < 18.43	189	177

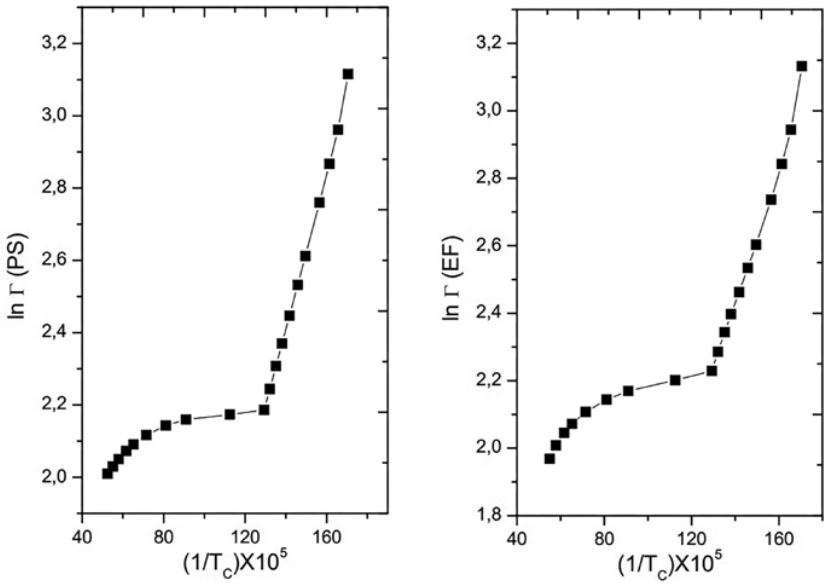

Fig. 4. Calculated damping constant (Γ_{SP}) as a function of the reciprocal temperature at room temperature to extract the activation energy U (Eq. 8) for the (a) PS (b) and EF models (Table 2) within the pressure intervals indicated in ZrO_2. Curve is shown as guide to the eye

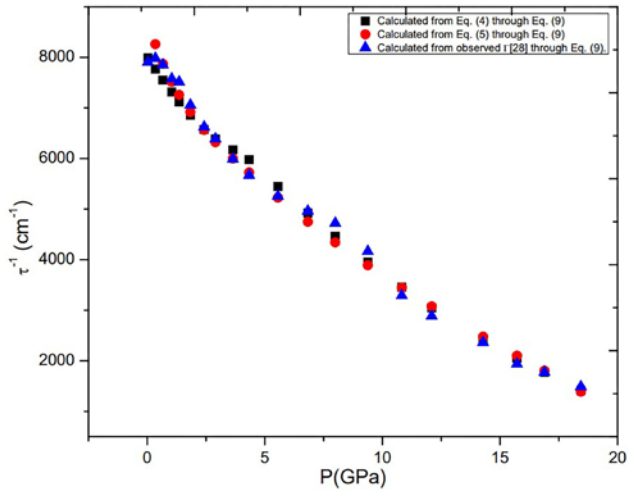

Fig. 5. Pressure dependency of the inverse relaxation time for the soft E_g mode in ZrO_2 according to Eq. (9)

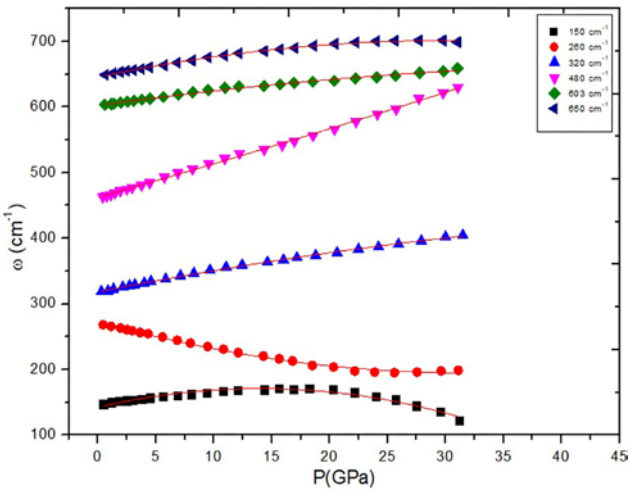

Fig. 6. The observed [28] frequencies for the 150, 260, 320, 480, 602, and 650 cm^{-1} Raman modes in ZrO_2 as a function of pressure according to Eq. (16)

The fitting parameters a_0 a_1, a_2 of the Raman frequency ω and b_0, b_1, b_2 of the volume V were tabulated in Tables 3 and 4, respectively, in the pressure intervals indicated.

Figure 8 shows our computed values of the isothermal Grüniesen parameter of the Raman modes in zirconia as a function of pressure.

3.2 Prediction of the linewidth as a function of temperature

The pressure dependence of the linewidth of the soft E_g mode at 260 cm^{-1} in ZrO_2 can be analyzed near phase transition pressure (P_C) using a power-law relationship as follows:

$$\Gamma = A\left(\frac{P}{P_C - P}\right)^{2\beta} \quad (18)$$

Here β and A are the critical exponent and the amplitude, respectively. This relationship describes the divergence trend of linewidth at critical pressure P_C. By taking the logarithm of the both sides, Eq. (18) becomes

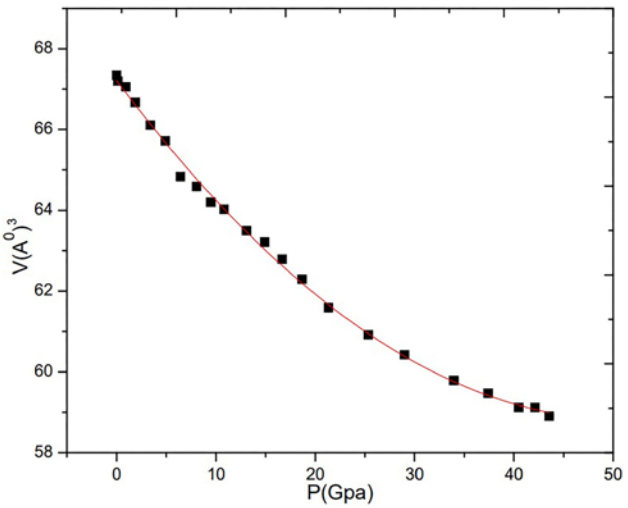

Fig. 7. The observed volume data [26] of ZrO_2 as a function of pressure according to Eq. (17)

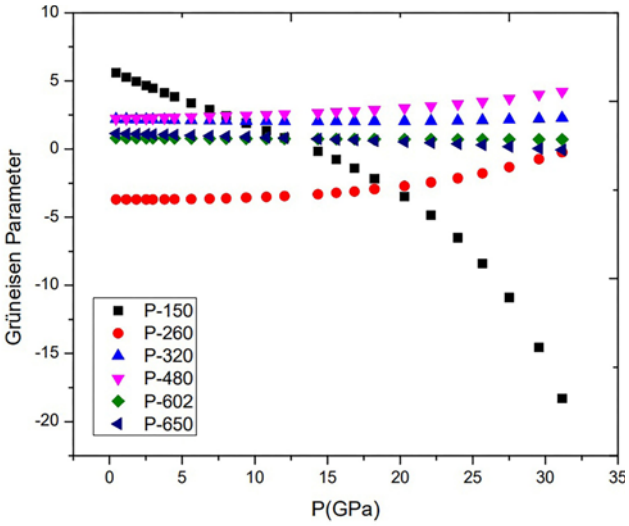

Fig. 8. Isothermal Grüneisen parameter γ_T of the Raman modes in ZrO_2 via Eq. (11)

Table 3. The values of the fitting parameter of Eq. (16) for the Raman modes in ZrO_2 within the pressure interval $0 \leqslant P \leqslant 40$ GPa using the observed Raman data [28]

Frequencies T = 298 K	a_0 (cm^{-1})	a_1 (cm^1/GPa)	a_2 (cm^1/Gpa^2)
150 cm^{-1}	142.55	4.06	−0.15
260 cm^{-1}	273.08	– 4.93	0.08
320 cm^{-1}	318.35	3.47	−0.02
480 cm^{-1}	462.18	5.02	0.01
602 cm^{-1}	602.49	2.41	−0.02
650 cm^{-1}	645.81	3.67	−0.06

Table 4. The values of the fitting parameters of Eq. (17) for the observed [26] cell volume in ZrO_2

Cell Volume (Å^3)	b_0 (Å^3)	b_1 (Å^3/GPa)	b_2 (Å^3/(GPa)^2)	Pressure Interval (GPa)
ZrO_2	67.21242	-0.32874	0.00322	$0 < P < 50$

$$\ln\Gamma = \ln A + 2\beta \ln\left(\frac{P}{P_C - P}\right) \tag{19}$$

The observed data for the Raman linewidth at different pressures in ZrO_2 can be utilized to predict the temperature-dependent behavior of this E_g soft Raman mode. For this reason, we first analyzed the observed linewidth [28] for both (M) – (T-II) and (O-I) – (O-II) transitions according to Eq. (19), as given in Fig. 9.

Our deduced values of the critical exponent β and the amplitude A were tabulated in Table 5.

Eqs. (13) and (15) which were obtained from the T-P phase diagram for both monoclinic (M) – tetragonal II (T-II) and orthorhombic I (O-I) – orthorhombic II (O-II) transitions (Fig. 2),respectively, are inserted into Eq. (19) to yield

$$\Gamma = A\left(\frac{3.85 - 0.0019T}{P_C + 0.0019T - 3.85}\right)^{2\beta} \tag{20}$$

and

$$\Gamma = A\left(\frac{21.8 - 0.0057T}{P_C + 0.0057T - 21.8}\right)^{2\beta} \tag{21}$$

where the transition pressures P_C at room temperature (~300 K) were 3.3 and 20.1. GPa, respectively, for the (M) – (T-II) and (O-I) – (O-II) transitions, respectively, as stated before. Thus, we were able to calculate the linewidth as a function of temperature through Eqs. (20) and (21) by using our extracted values of critical exponent β and the amplitude A (Table 5). Fig. 10 shows our predicted values of the linewidth Γ. the E_g mode (260 cm^{-1}) for the two transitions indişcated at various temperatures.

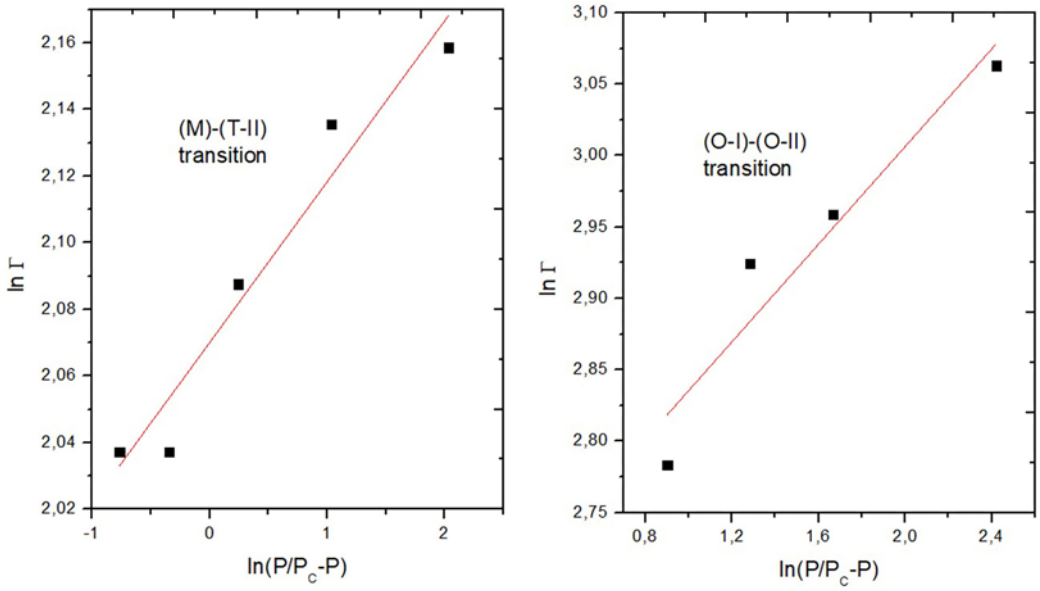

Fig. 9. Linewidth of the observed [28] soft Raman E_g mode (260 cm^{-1}) as a function of pressure in the ln-ln scale according to Eq. (19)

Table 5. Values of the critical exponent β and the amplitude A according to Eq. (19) within the pressure ranges at room temperature for the phases indicated in ZrO_2

Phases	β	A (cm^{-1})	P_C (GPa)	Pressure interval (GPa)
(M)- (T-II)	0.024	7.92	3.3	1.0 < P < 2.9
(O-I)- (O-II)	0.085	14.35	20.1	14.3 < P < 18.4

4. Discussion

The molecular field theory [38] provides an acceptable description of the order parameter S as a function of temperature, and it is given as

$$S \approx \begin{cases} 1-\exp\left(-\dfrac{2T_C}{T}\right) & T \ll T_C \\ \left\{3\left(1-\dfrac{T}{T_C}\right)\right\}^{1/2} & 0<(T_C-T)<T_C \\ 0 & T_C<T \end{cases} \quad (22)$$

on the other hand, based on the Cohran's theory [46] the soft mode behaviour can be described according to the relation

$$\omega \sim (T_C - T)^{\frac{1}{2}} \quad (23)$$

where ω represents the soft mode frequency. Once we know the relations for the pressure P and the transition temperature T_C from the P-T phase diagram of any ferroelectric material, it is possible to calculate the order parameter S and the soft mode frequency ω as a function of pressure. Therefore, soft mode ferroelectric transitions can be characterized by the molecular field theory (Eq. 22) and the Cohran's theory (Eq. 23), where T replaces P, with a power-law of $\omega^2 = a(T_C - T)^b$ with b =1 [47]. A spectral

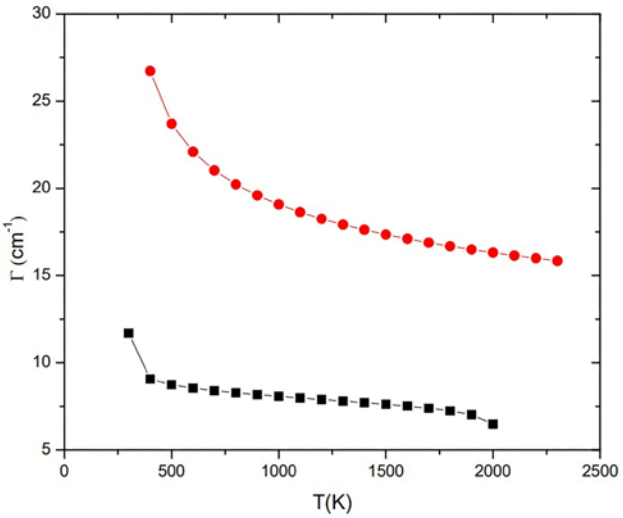

Fig. 10. Our predicted linewidth for the (M)-(T-II) and (O-I)-(O-II) transitions in ZrO_2 according to Eqs. (20) and (21), respectively, as a function of temperature for the soft E_g mode at 260 cm^{-1}. Curve is shown as a guide to the eye

exchange between the two low frequencies (at 150 and 260 cm^{-1}) has been observed experimantally in ZrO_2 [28]. The gradual decay of the E_g mode at 260 cm^{-1}, which softens with increasing pressure, both before and after it hybridized with the other E_g mode at 150 cm^{-1}, has been represented by a Landau type empirical formula of $\omega^2 = 1916\ (38.03 - P)^{0.945}$ [28]. Thus, the frequency (ω) of the soft E_g mode in ZrO_2 can be regarded as an order parameter (S), as we examined here, because this empirical formula is almost in the same functional form as Eq. (22) with the critical exponent b = 1/2 for the order parameter. Consequently, this ratio of the frequency squared $(\omega / \omega_{max})^2$ was obtained between 0.50 and 1.0 as the order parameter squared (S^2) which decreased with increasing pressure toward the transition pressure in this crystal, as given in Fig. 1.

The pressure-temperature phase diagram of ZrO_2 and the ratio of the frequency $(\omega / \omega_{max})^2$ represents the squared order parameter S^2 (Eq. 12), were used for the pressure dependence of the linewidth Γ for the soft Raman E_g mode at 260 cm^{-1} by the PS (Eq. 4) and EF (Eq. 5) models. In particular, the linear P-T_C relations for the M – T II (Eq. 13), T I – T II (Eq. 14) and the orthorhombic O I – O II (Eq. 15) transitions in ZrO_2 were determined, as stated before. Our calculations indicate that the P-T_C relations (Eqs. 13, 14 and 15) within the pressure intervals of 0 < P(GPa) < 2, 2 < P(GPa) < 16 and 16 < P(GPa) < 20, respectively, describe the increasing trend of the linewidth Γ as the pressure increases, as observed experimentally [28]. Thus, Eqs. (13), (14) and (15) were inserted in both the PS (Eq. 4) and EF (5) models, within the indicated pressure intervals above, to estimate the linewidth of this soft E_g mode in ZrO_2 as a function of pressure. Our computed values of Γ through the PS and EF models were then fitted to the recorded data [28] and the fitting parameters of Eqs. (4) and (5) were determined within the pressure intervals, as provided in Table 1. Fig. 3 shows our obtained values of Γ from both PS and EF models as a function of pressure. The observed data [28] were also given here, for comparison. We can conclude that the two models studied here adequately describe the observed data within the pressure intervals of the observed data.

Our estimated values of Γ (Fig. 3) were then used to calculate the values of the activation energy U according to Eq. (8), as given in Table 2 for the pressure intervals indicated. Note that all extracted values of U are all negative. This is the expected result because of that pressure and transition temperature are inversely proportional. As the pressure increases, the transition temperature drops as seen in Figure 2 and previously reported [25]. We also investigated the pressure dependency of the inverse relaxation time τ^{-1} for the soft Eg mode (Fig. 5). The inverse relaxation time decreases with increasing pressure, as predicted by the PS and EF models. This is consistent with the growing linewidth (broadening) as pressure grows and relaxation time approaches the transition pressure Pc.

Once we get the pressure dependence of the Raman frequency (Eq. 16) for the 150, 260, 320, 480, 602, and 650 cm^{-1} Raman modes in ZrO_2 (Fig.6 and Table3), we were able to calculate the isothermal Grüneisen parameter γ_T of the Raman modes in ZrO_2 via Eq. (11). For this calculation of γ_T, the observed volume data [26] of ZrO_2 were analyzed as a function of pressure (Fig. 7) according to Eq. (17), as also given in Table 4. Our results for the isothermal Grüneisen parameter γ_T were represented in Fig. 8. One can see very easily that while the values of γ_T for the 150 cm^{-1} band sharply drops as pressure rises, it only slightly increases for the soft E_g (260 cm^{-1}) band and also the others (320, 480, 602, and 650 cm^{-1}).

Finally, we presumed that the temperature dependence of the linewidth Γ of the soft E_g mode can be predicted from the pressure dependence of its linewidth Γ according to to a power-law formula (Eq. 18). Similar treatment has been applied by Yurtseven and Senol [48] for an internal mode in the solid phases of benzene. For this reason, we first analyzed the linewdith of this soft mode as a function of pressure in the ln-ln scale according to Eq. (19), as given in Fig. 9. From this graph we extracted values of β and A with the the P - T_C relation (Eqs. 13 and 15) for the (M)-(T-II) and (O-I)- (O-II) transitions, respectively, have been inserted in Eq. (18) to get Eqs. (20) and (21). This equation specifies the temperature evolution of the linewidth. Our predicted values of Γ for this soft E_g mode at 260 cm^{-1} are given

in Fig. 10. It can be compared with experimental data when available in the literature.

5. Conclusions

Some properties such as the linewidth, frequency, activation energy, inverse relaxation time and the isothermal Grüneisen parameter of the soft Raman E_g mode in ZrO_2 were calculated and explored as a function of pressure. The PS and EF models, which take into account pseudospin-phonon interactions through the Ising model, adequately described the pressure dependence of the reported linewidth of this E_g mode. In addition, a trial (power-law formula) was employed to determine the temperature dependency of this soft mode's linewidth based on its pressure dependence, which can also be examined with the observed data.

Author Contributions

Some of the content of this manuscript is based on Nazan Kara's Ph.D. thesis. The thesis, titled "Phenomenological Approaches on the Phase Transition Mechanisms of Some Ferroelectric Materials," is supervised by Hamit Yurtseven and co-supervised by Ali Kiracı. The authors (Nazan Kara, Ali Kiraci and Hamit Yurtseven) confirm the sole responsibility for the conception of the study, presented results and manuscript preparation.

Conflict of interest

The corresponding author state that there is no confict of interest.

References

1. Gorelov V. P. High-temperature phase transitions in ZrO_2. *Physics of the Solid State* 2019;61: 1288–1293. https://doi.org/10.1134/S1063783419070096

2. Terki R., Bertrand G., Aourag H., Coddet C. Structural and electronic properties of zirconia phases: a FP-LAPW investigations. *Materials Science in Semiconductor Processing*. 2006;9:1006–1013. https://doi.org/10.1016/j.mssp.2006.10.033

3. Ohtaka O., Yamanaka T., Yagi T. New high-pressure and -temperature phase of ZrO_2 above 1000 °C at 20 GPa. *Physical Review B*. 1994;49: 9295–9298. https://doi.org/10.1103/PhysRevB.49.9295

4. Haines J., Léger J. M., Atouf A. Crystal structure and equation of state of cotunnite-type zirconia. *Journal of the American Ceramic Society*. 1995;78: 445–448. https://doi.org/10.1111/j.1151-2916.1995.tb08822.x

5. Arashi H., Yagi T., Akimoto S., Kudoh Y. New high-pressure phase of ZrO_2 above 35 GPa. *Physical Review B*. 1990;41:4309–4313. https://doi.org/10.1103/PhysRevB.41.4309

6. Desgreniers S., Lagarec K. High-density ZrO_2 and HfO_2: Crystalline structures and equations of state. *Physical Review B*. 1999;59: 8467–8472. https://doi.org/10.1103/PhysRevB.59.8467

7. Haines J., Léger J. M., Hull S., ... da Jornada J. A. H. Characterization of the cotunnite-type phases of zirconia and hafnia by neutron diffraction and Raman spectroscopy. *Journal of the American Ceramic Society*. 1997;80: 1910–1914. https://doi.org/10.1111/j.1151-2916.1997.tb03073.x

8. Ohtaka O., Fukui H., Funakoshi K., Utsumi W., Irifune T., Kikegawa T. Phase relations and EOS of ZrO_2 and HfO_2 under high-temperature and high-pressure. *High Pressure Research*. 2002;22: 221–226. https://doi.org/10.1080/08957950211347

9. Léger J. M., Tomaszewski P. E., Atouf A., Pereira A. S. Pressure-induced structural phase transitions in zirconia under high pressure. *Physical Review B*. 1993;47: 14075–14083. https://doi.org/10.1103/physrevb.47.14075

10. Howard C. J., Hill R. J., Reichert B. E. Structures of ZrO_2 polymorphs at room temperature by high-resolution neutron powder diffraction. *Acta Crystallographica Section B Structural Science*. 1988;44: 116–120. https://doi.org/10.1107/S0108768187010279

11. Teufer G. The crystal structure of tetragonal ZrO_2. *Acta Crystallographica*. 1962;15: 1187. https://doi.org/10.1107/S0365110X62003114

12. Yoshimura M. Phase stability of zirconia. *American Ceramic Society Bulletin*. 1988;67: 1950–1955.

13. Lityagina L. M., Kabalkina S. S., Pashkina T. A., Khzyainov A. Polymorphism of ZrO_2 at high pressures. *Fizika Tverdogo Tela*. 1978;20: 3475–3477. (In Russ.)

14. Liu L. New high pressure phases of ZrO_2 and HfO_2. *Journal of Physics and Chemistry of Solids*. 1980;41:331–334. https://doi.org/10.1016/0022-3697(80)90205-X

15. Leger J. M., Atouf A., Tomaszewski P. E., Pereira A. S. Pressure-induced structural phase transitions in zirconia under high pressure. *Physical Review B*. 1993;47: 14075–14083. https://doi.org/10.1103/PhysRevB.47.14075

16. Zhao X., Vanderbilt D. Phonons and lattice dielectric properties of zirconia. *Physical Review B*. 2002;65: 075105. https://doi.org/10.1103/PhysRevB.65.075105

17. Sternik M., Parlinski K. Lattice vibrations in cubic, tetragonal, and monoclinic phases of ZrO_2. *The Journal of Chemical Physics*. 2005;122: 064707. https://doi.org/10.1063/1.1849157

18. Fadda G., Colombo L., Zanzotto G. First-principles study of the structural and elastic properties of zirconia. *Physical Review B*. 2009;79: 214102. https://doi.org/10.1103/PhysRevB.79.214102

19. Milman V., Perlov A., Refson K., Clark S. J., Gavartin J., Winkler B. Structural, electronic and vibrational properties of tetragonal zirconia under pressure: a density functional theory study. *Journal of Physics: Condensed Matter*. 2009;21: 485404. https://doi.org/10.1088/0953-8984/21/48/485404

20. Parlinski K., Li Z. Q., Kawazoe Y. First-principles determination of the soft mode in cubic ZrO_2. *Physical Review Letters*. 1997;78: 4063–4066. https://doi.org/10.1103/PhysRevLett.78.4063

21. Souvatzis P., Rudin S. P. Dynamical stabilization of cubic ZrO_2 by phonon-phonon interactions: Ab initio calculations. *Physical Review B*. 2008;78: 184304. https://doi.

org/10.1103/PhysRevB.78.184304

22. Caravaca M. A., Miño J. C., Pérez V. J., Casali R. A., Ponce C. A. Ab initio study of the elastic properties of single and polycrystal TiO_2, ZrO_2 and HfO_2 in the cotunnite structure. *Journal of Physics: Condensed Matter*. 2009;21: 015501. https://doi.org/10.1088/0953-8984/21/1/015501

23. Rignanese G. M., Detraux F., Gonze X., Pasquarello A. First-principles study of dynamical and dielectric properties of tetragonal zirconia. *Physical Review B*. 2001;64: 134301. https://doi.org/10.1103/PhysRevB.64.134301

24. Fadda G., Zanzotto G., Colombo L. First-principles study of the effect of pressure on the five zirconia polymorphs. I. Structural, vibrational, and thermoelastic properties. *Physical Review B*. 2010;82: 064105. https://doi.org/10.1103/PhysRevB.82.064105

25. Block S., Jornada J. A., Piermarini G. J. Pressure-temperature phase diagram of zirconia. *Journal of the American Ceramic Society*. 1985;68: 497–499. https://doi.org/10.1111/j.1151-2916.1985.tb15817.x

26. Bouvier P., Djurado E., Lucazeau G., Le Bihan T. High-pressure structural evolution of undoped tetragonal nanocrystalline zirconia. *Physical Review B*. 2000;62: 8731–8737. https://doi.org/10.1103/PhysRevB.62.8731

27. Park J. H., Bang I. H., Lee S. J. Phase transition and thermal expansion behavior of zirconia setter fabricated from fused CaO stabilized zirconia. *Journal of the Korean Ceramic Society*. 2019;56: 184–190. https://doi.org/10.4191/kcers.2019.56.2.08

28. Bouvier P., Lucazeau G. Raman spectra and vibrational analysis of nanometric tetragonal zirconia under high pressure. *Journal of Physics and Chemistry of Solids*. 2000;61: 569–578. https://doi.org/10.1016/S0022-3697(99)00242-5

29. Li C. W., Smith H. L., Lan T., ... Fultz B. Phonon anharmonicity of monoclinic zirconia and yttrium-stabilized zirconia. *Physical Review B*. 2015;91: 144302. https://doi.org/10.1103/PhysRevB.91.144302

30. Bouvier P., Godlewski J., Lucazeau G. A Raman study of the nanocrystallite size effect on the pressure–temperature phase diagram of zirconia grown by zirconium-based alloys oxidation. *Journal of Nuclear Materials*. 2000;300: 118–126. https://doi.org/10.1016/S0022-3115(01)00756-5

31. Kiraci A., Yurtseven H. Pressure-dependent Raman modes near the cubic-tetragonal transition in strontium titanate. *Journal of the American Ceramic Society*. 2018;101: 1344–1355. https://doi.org/10.1111/jace.15279

32. Kiraci A., Yurtseven H. Damping constant calculated as a function of temperature for the tetragonal Raman mode close to the paraelectric-ferroelectric transition in $BaTiO_3$. *Ferroelectrics*. 2013;450: 93–98. https://doi.org/10.1080/00150193.2013.838500

33. Kiraci A., Yurtseven H. Damping constant and the relaxation time calculated for the lowest-frequency soft mode in the ferroelectric phase of $Cd_2Nb_2O_7$. *Optik*. 2016;127: 11497. https://doi.org/10.1016/j.ijleo.2016.09.023

34. Yurtseven H., Kiraci A. Damping constant (linewidth) and the relaxation time of the brillouin LA mode for the ferroelectric-paraelectric transition in $PbZr_{1-x}Ti_xO_3$. *IEEE Transactions on Ultrasonics, Ferroelectrics, and Frequency Control*. 2016;63: 1647–1655. https://doi.org/10.1109/TUFFC.2016.2572044

35. Kara N., Kiraci A., Yurtseven H. Phenomenological approaches on the Nd^{3+} doped ferroelectric $LaBGeO_5$. *Ferroelectrics*. 2021;572: 13–26. https://doi.org/10.1080/00150193.2020.1868869

36. Kara N., Kiraci A., Yurtseven H. Calculation of the spin-lattice relaxation time and the activation energy near the IV–III phase transition in pyridinium fluorosulfonate $(C_5NH_6)FSO_3$. *Ferroelectrics*. 2022;589: 45–54. https://doi.org/10.1080/00150193.2022.2061216

37. Yamada Y., Mori N., Noda Y. A microscopic theory on the phase transitions in NH_4Br -an ising spin phonon coupled system. *Journal of the Physical Society of Japan*. 1972;32: 1565–1576. https://doi.org/10.1143/JPSJ.32.1565

38. Matsushita M. Anomalous temperature dependence of the frequency and damping constant of phonons near T_λ in ammonium halides. *The Journal of Chemical Physics*. 1976;65: 23–29. https://doi.org/10.1063/1.432804

39. Laulicht I., Luknar N. Internal-mode line-broadening by proton jumps in KH_2PO_4. *Chemical Physics Letters*. 1976;47: 237–240. https://doi.org/10.1016/0009-2614(77)80008-0

40. Schaack G., Winterfeldt V. Temperature behaviour of optical phonons near *T*c in triglycine sulphate and triglycine selenate, II. Evidence of non-linear pseudospin-phonon interaction. *Ferroelectrics*. 1977;15: 35–41. https://doi.org/10.1080/00150197708236718

41. Laulicht I. The drastic temperature broadening of hard mode Raman lines of ferroelectric KDP type crystals near Tc. *Chem. Solids*. 1978; 39:901-906. https://doi.org/10.1016/0022-3697(78)90153-1

42. Yurtseven H., Karacali H. Temperature dependence of the damping constant and the order parameter close to the λ phase transitions in ammonium halides. *Spectrochimica Acta Part A: Molecular and Biomolecular Spectroscopy*. 2006;65: 421–427. https://doi.org/10.1016/j.saa.2005.10.054

43. Lahajnar G., Blinc R., Zumer S. Proton spin-lattice relaxation by critical polarization fluctuations in KH_2PO_4. *Physics of Condensed Matter*. 1974;18: 301–316. https://doi.org/10.1007/BF01464399

44. Rakov A. V. The influence of intermolecular interaction on line width in the Raman spectra of liquids. *Optics and Spectroscopy*. 1959;7: 128–131.

45. Bartoli F. F., Litovitz T. A. Raman scattering: orientational motions in liquids. *The Journal of Chemical Physics*. 1972;56: 413–425. https://doi.org/10.1063/1.1676883

46. Cochran W. Crystal stability and the theory of ferroelectricity. *Advances in Physics*. 1960;9: 387–423. https://doi.org/10.1080/00018736000101229

47. Kittel C. *Introduction to solid state physics*. Wiley, New York; 1976.

48. Yurtseven H., Senol M. G. Temperature and pressure dependence of the linewidth for an internal mode in the solid phases of benzene. *Acta Physica Polonica A*. 2013;124: 698–701. https://doi.org/10.12693/APhysPolA.124.698

Information about the authors

Nazan Kara, PhD in Physics, Graduated from Middle East Technical University (Ankara, Türkiye).
https://orcid.org/0000-0002-9721-6224
nazankara0511@gmail.com

Ali Kiraci, Professor, Intercurricular Courses Department, Cankaya University (Ankara, Türkiye).
https://orcid.org/0000-0003-4067-1004
akiraci@cankaya.edu.tr

Hamit Yurtseven, Professor, Department of Computer Engineering, Baskent University (Ankara, Türkiye).
https://orcid.org/0000-0002-7745-6490

Received October 20, 2025; approved after reviewing February 5, 2026; accepted for publication February 16, 2026; published online September 25, 2026.